LETTER

Realization of spinful metaphotonic stokes skyrmions

IOP Publishing
Letters
Journal of Optics
J. Opt. **26** (2024) 09LT01 (5pp)
https://doi.org/10.1088/2040-8986/ad699e

Letter

Realization of spinful metaphotonic stokes skyrmions

Tianyue Li[1,2], Mengjiao Liu[1,2], Chen Chen[1,2,3], Xingyi Li[4], Jiahao Hou[1,2], Xing Yang[1,2], Shuming Wang[1,2,5,*] and Shining Zhu[1,2,5]

[1] National Laboratory of Solid-State Microstructures, School of Physics, College of Engineering and Applied Sciences, Nanjing University, Nanjing 210093, People's Republic of China
[2] Collaborative Innovation Center of Advanced Microstructures, Nanjing University, Nanjing 210093, People's Republic of China
[3] Department of Physics, Department of Electrical Engineering, City University of Hong Kong, Tat Chee Avenue, Kowloon, Hong Kong Special Administrative Region of China, People's Republic of China
[4] College of Optical Science and Engineering, Zhejiang University, Hangzhou 310027, Zhejiang, People's Republic of China
[5] Key Laboratory of Intelligent Optical Sensing and Manipulation Ministry of Education, Nanjing 210093, People's Republic of China

E-mail: wangshuming@nju.edu.cn

Received 4 June 2024, revised 25 July 2024
Accepted for publication 31 July 2024
Published 7 August 2024

Abstract

Topologically protected skyrmion textures of light have garnered significant attention due to their potential applications in next-generation high-density data storage and logic devices. However, achieving compact and tunable on-chip skyrmion modes remains a formidable challenge. In this work, we present a novel approach empowered by birefringent metasurfaces to generate and manipulate spin-multiplexed photonic skyrmion textures. By encoding independent phase profiles onto orthogonal spin states, we observe the emergence of anti-skyrmions and skyrmioniums via Stokes parameter measurements, elucidating their distinct topological characteristics. This spin-multiplexed metasurface platform not only facilitates high-dimensional multiplexing but also enables the miniaturization of topological quasi-particles, offering promising prospects for applications in optical memory, information processing, and communications.

Keywords: metaphotonic skyrmion, topological light field, multidimensional metasurface, topological photonics

1. Introduction

Topological photonics introduces a novel degree of freedom (DoF) distinct from frequency, wavevector, polarization, and phase [1, 2]. It is inspired by mathematical methods and concepts from topology and geometry to reveal new physics hidden within inhomogeneous electromagnetic media or structured light fields. In periodic microstructures like photonic crystals and metamaterials, variations in the periodic potential well are accompanied by the property of topological protection, such as unidirectional propagation, immunity to backscattering, and defect states [3, 4]. As a result, photonic topological insulators emerge, typically characterized by features in momentum space and described by topological invariants such as Chern number, Wilson loop, and Zak phase [5]. Parallelly, topology is applicable to structured classical or quantum field distributions in optics and photonics, such as vortex and vector fields [6, 7], optical knots [8], Möbius strips [9]. Over the past decade, topological photonics has rapidly evolved, benefiting

* Authors to whom any correspondence should be addressed.

from its more flexible structural designs compared to traditional electronics, and expanding into other parameter spaces such as synthetic dimensions [10], non-Hermitian physics [11], and skyrmion textures [12]. skyrmion textures, observed in liquid crystal [13] or Bose-Einstein condensate [14], originating from unified field theories of mesons and baryons interactions, are topologically protected quasi-particle spin structures with excellent properties like high stability, fast mobility, and small size, making them promising candidates for solid-state storage to replace traditional magnetic domains, potentially serving as information carriers for next-generation high-speed, high-density, low-power, non-volatile magnetic storage and logic devices [12].

Photonic skyrmion textures could exist depending on different parameters in the spatiotemporal light field [15–17], evanescent wave [18–21], and momentum space [22, 23]. For spatiotemporal structural light, skyrmion textures can be described by the Stokes parameters [24–26], necessitating the generation of vector optical fields with broken symmetries, typically achieved through spatial light modulators followed by spatial filtering [15]. However, to further shrink the pixel of skyrmion texture, simplify the complexity of the optical system, and increase tunability in multidimensions, an integrated compact nanophotonic device is required. Metasurfaces, as highly suitable flat devices, have been turned out that it has great potential in the fields of optical imaging and display [27–29], structured light generation and manipulation [30–34], optical micromanipulation [35–37], nonlinear and quantum optics [38–40], etc.

In this work, we theoretically realize and experimentally demonstrate spin-multiplexed generation and manipulation of skyrmions using an exotic spinful metasurface, namely the Skyr-plate. By exciting spin-up and spin-down states, we generate anti-skyrmions and skyrmioniums by not only compressing the pixels of skyrmions but also controlling by spin characteristics, allowing high-dimensional multiplexing. This work represents a significant step forward in combining topological quasi-particles with metamaterials, advancing the miniaturization of skyrmions and providing insights for the development of future state-of-the-art applications.

2. Result

Figure 1(a) illustrates schematically two types of skyrmion textures controlled by incident spin states based on the individual metasurface. Upon excitation with spin-up, an anti-type skyrmion is generated, whereas upon switching to spin-down, anti-type skyrmioniums are observed. Subsequent sections will provide a detailed explanation of their formation and experimental principles.

2.1. Formation principle of photonic skyrmion

Based on the classification of skyrmions in different parameter spaces, we have generated a far-field pattern based on the Stokes vector $\boldsymbol{S} = (S_1, S_2, S_3)$, therefore the construction of customized spatial mode vector beams is essential. Generally,

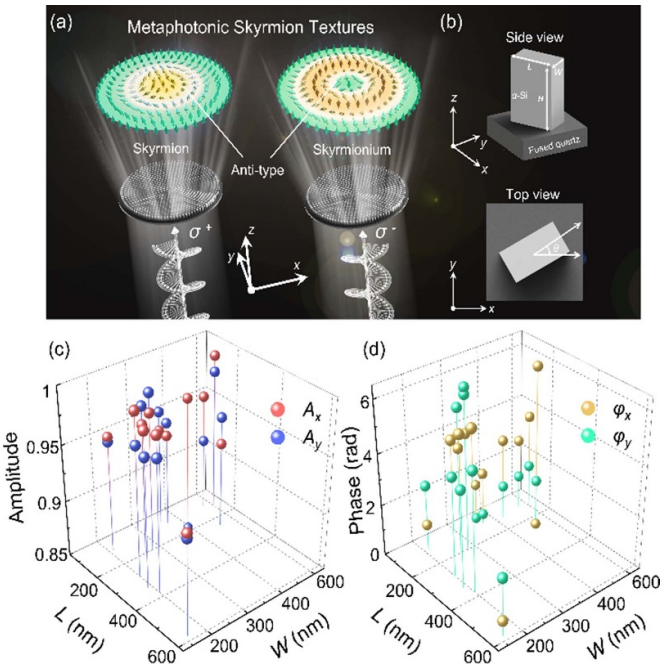

Figure 1. (a) Schematic illustration of metaphotonic skyrmions. Anti-type skyrmions and skyrmionium are generated by activating orthogonal CP states from above and below. (b) Schematic diagram of α-Si meta-atoms grown on fused quartz. (c) Library of selected meta-atoms depicting their amplitudes and phase shifts along the fast and slow axes.

the geometric phase in the circular polarization (CP) basis can carry a conjugate phase profile. For instance, the spatial mode of a Q-plate can be expressed as [41]:

$$\mathrm{E}_{\mathrm{out}} = \mathrm{e}^{\mathrm{i}l_0\psi}\,|R\rangle L| + \mathrm{e}^{-\mathrm{i}l_0\psi}\,|L\rangle R| \tag{1}$$

where l_0 denotes the topological charge of the vortex beam, $\psi = \arctan(y/x)$ is the azimuthal angle. However, since the generation of skyrmions requires the breaking of symmetry in the eigenmodes, it is necessary to introduce an additional reference phase as an extra DoF of the geometric phase, modifying equation (1) to [42]:

$$\mathrm{E}_{\mathrm{out}} = \mathrm{e}^{\mathrm{i}l_1\psi}\,|R\rangle\langle L| + \mathrm{e}^{\mathrm{i}l_2\psi}\,|L\rangle\langle R| \tag{2}$$

where $l_{1,2}$ represent unrelated topological charges. Although J-plate has been demonstrated to achieve independent orbital angular momentum of light with different topological charges by illuminating CP bases of a plane wave at the metasurface, thereby realizing skyrmion fields under linear polarization (LP) incidence, they are limited to generating only one type of skyrmion at a time and lack the capability for multidimensional Multiplexing. Here, we introduce a novel method to enhance the DoFs in spin states, enabling the generation of versatile skyrmion textures. This Skyr-plate fundamentally diverges from the approach of generating skyrmions using J-plates, allowing for the manipulation of skyrmion textures via spin control.

2.2. Metasurface implement

To manipulate the spin states incident on the metasurface, the construction of composite-phase birefringent meta-atoms needs to be addressed. In the classical representation, the spin angular momentum (SAM) of light aligns with the orthogonal CP states of the wave. Consequently, according to the effective medium theory, the meta-atoms exhibit a significant contrast in their refractive indices for orthogonal polarizations. Thus, the Jones matrix can be employed to describe their complex transmission properties as follows [42–46]:

$$J(x,y) = R(\theta)\begin{bmatrix} T_o e^{i\varphi_o(x,y)} & 0 \\ 0 & T_e e^{i\varphi_e(x,y)} \end{bmatrix} R(-\theta) \quad (3)$$

where (T_o, T_e) and (φ_o, φ_e) represent the amplitude of transmission and phase shifts along the ordinary and extraordinary axes of meta-atoms, respectively, and $R(\theta)$ is the rotation matrix of the metasurfaces. Here, $T_o = T_e$ phase difference is defined by $\delta = \varphi_o - \varphi_e$ and reference phase shift $\varphi_r = (\varphi_o + \varphi_e)/2$ for convenience. The Jones matrix can be simplified as follows:

$$J(x,y) = Te^{i\phi_r(x,y)}\begin{pmatrix} \cos\frac{\delta}{2} + i\cos 2\theta \sin\frac{\delta}{2} & -i\sin 2\theta \sin\frac{\delta}{2} \\ -i\sin 2\theta \sin\frac{\delta}{2} & \cos\frac{\delta}{2} - i\cos 2\theta \sin\frac{\delta}{2} \end{pmatrix}. \quad (4)$$

For the incoming CP, the Jones matrix with CP bases $|L\rangle = \begin{bmatrix} 1 & -i \end{bmatrix}^T/\sqrt{2}$ and $|R\rangle = \begin{bmatrix} 1 & i \end{bmatrix}^T/\sqrt{2}$ can be simultaneously realized as cross-CP and co-CP channels, respectively, therefore, equation (4) can be expressed as follows:

$$J(x,y) = Te^{i\varphi_r(x,y)} \cdot \begin{bmatrix} \cos\left(\frac{\delta}{2}\right) & i\sin\left(\frac{\delta}{2}\right)e^{-i2\theta} \\ i\sin\left(\frac{\delta}{2}\right)e^{i2\theta} & \cos\left(\frac{\delta}{2}\right) \end{bmatrix}. \quad (5)$$

The phase difference δ governs not only the polarization states of both the incident and transmitted beams but also the associated phase profiles. By strategically selecting nanopillars with specific phase differences at various positions across the metasurface, the independent skyrmions with distinct spins can be achieved. In our implementation, the metasurface design is based on an amorphous silicon (α-Si) film deposited on fused quartz and arranged according to the geometric shape (L, W, H) and rotation angle (θ) of each meta-atom at working wavelength $\lambda = 1064$ nm, as depicted in figure 1(b). Figures 1(c) and (d) illustrate the chosen amplitudes and phase shifts of the meta-atoms, respectively, along with their structural parameters, as determined through finite-difference time-domain simulations with periodic length $\Lambda = 600$ nm. When $\delta = \pi/2$, three distinct phase responses can be controlled for CP, where $\varphi_1 = \varphi_r$, $\varphi_2 = \varphi_r + 2\theta$, and $\varphi_3 = \varphi_r - 2\theta$. Through this approach, we can now employ vector beams to realize spin-activated skyrmions through their Stokes fields by setting $\varphi_r = l_r\psi$ and $\theta = l_0\psi/2$. To validate this methodology, we set $l_0 = 1$ and $l_r = 1$, corresponding to the topological textures of an anti-type skyrmion or skyrmionium. Samples were fabricated using mature fabrication techniques [47].

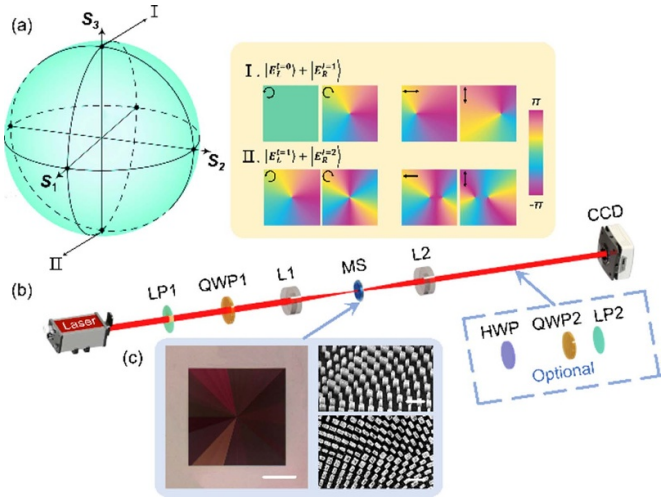

Figure 2. (a) The encoded phase profiles projected onto the Poincaré sphere, the regions of I and II on the Poincaré sphere represent the CP and LP components of encoded phase profiles, respectively. (b) The experimental setup, where LP denotes the linear polarizer, QWP denotes the quarter-wave plate, MS represents the metasurface, and L1 and L2 are lenses. (c) Optical microscopy (left, scale bar, 200 μm) and SEM (right, scale bar, 1 μm) characterizations of the sample.

2.3. Experimental demonstration

The experimental setup for measuring the designed Skyr-plate is illustrated in figure 2(b). The filtered continuous wave (CW) laser, operating at a wavelength of 1064 nm, passing through a set of polarizers, is focused by a convex lens, and then enters the metasurface sample whose optical microscopy and scanning electronic microscopy (SEM) are shown in figure 2(c), respectively. After transmission through a collection lens and several optional elements, the image is captured by a CCD camera. When the incident light is right circularly polarized (RCP), as encoded in figure 2(a), the output light emerging from the metasurface contains both left circularly polarized (LCP) and RCP components. Without performing an additional polarization filtering process, the interference between these components generates skyrmions, as shown in figure 3.

Figure 3(a) presents the simulated and experimental results in real space, while figures 3(b) and (c) display the corresponding Stokes parameters that can be measured by the optional elements, enabling the reconstruction through the measurement and recording of different polarization states by follow [15]:

$$\begin{aligned} S_0 &= I_H + I_V, S_1 = 2I_H - S_0 \\ S_2 &= 2I_D - S_0, S_3 = 2I_R - S_0 \end{aligned} \quad (6)$$

where $I_{H,V,D,R}$ are measured intensity under horizontal, vertical, 45° LP and RCP states. The simulated and experimental results of the skyrmion texture under RCP excitation in Stokes space are shown in figures 3(d) and (e). Although there are errors caused by the spherical wave effect provided by the lens during recording, these do not impact the topological texture, whose invariant can be calculated using the following formula [12]:

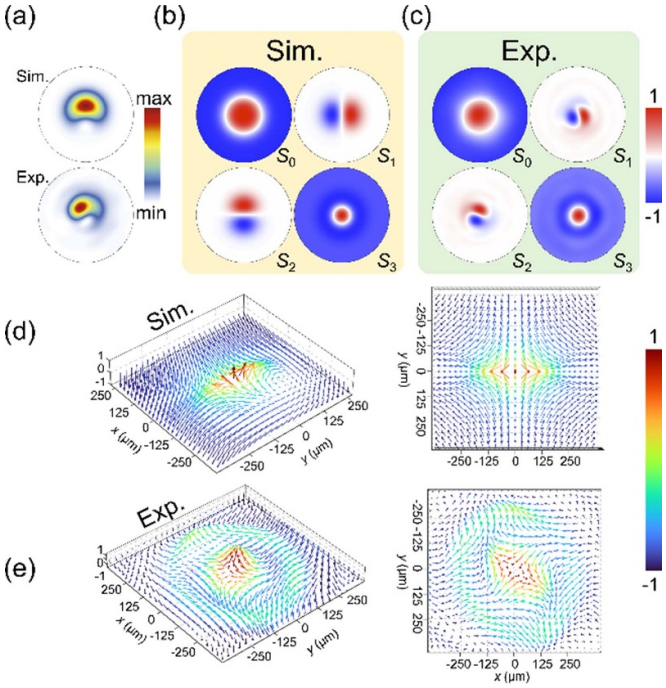

Figure 3. Skyrmion with RCP incidence. (a) Transverse pattern and its corresponding simulations (b) and experimental (c) Stokes parameter results. (d) and (e) depict the calculated saddle-like skyrmion textures.

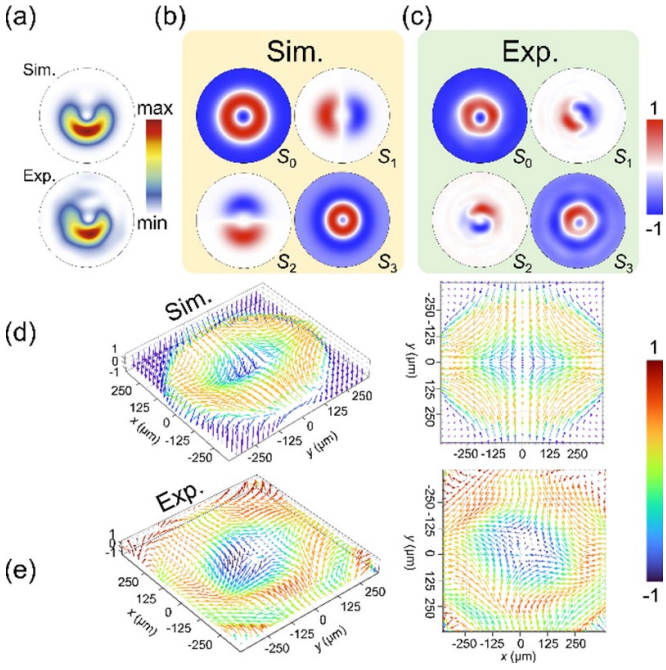

Figure 4. Skyrmionium with LCP illumination. (a) The recorded light field with accompanying simulations (b) and experimental (c) Stokes parameter results. (d) and (e) show the calculated saddle-like skyrmionium textures.

$$s = \frac{1}{4\pi}\iint_{\Omega} \boldsymbol{S}\cdot\left(\frac{\partial \boldsymbol{S}}{\partial x}\times\frac{\partial \boldsymbol{S}}{\partial y}\right)\mathrm{d}x\mathrm{d}y \tag{7}$$

where $\boldsymbol{S}(x,\ y)$ represents the vector field to construct a skyrmion and Ω denotes the region to confine the skyrmion. In this case, $s=-1$. Additionally, the right panels of figures 3(d) and (e), which presents top-view images, distinctly reveal the saddle-like shape. According to the Poincaré-Hopf theorem, the topological invariant can be determined similarly [48]. Upon the incidence of LCP light, a skyrmionium is generated due to $\varphi_{\mathrm{out}} = |l=2\rangle|R\rangle + |l=1\rangle|L\rangle$. The captured images and the associated S parameters are shown in figures 4(a)–(c). Unlike a skyrmion, the skyrmionium oscillates radially from the exterior to the interior as shown in figures 4(d) and (e), with the center maintaining a saddle shape but its coupled state connecting two skyrmions with opposite polarities, leading to $s = 0$. The tuning parameters of skyrmions are not solely dependent on the topological charge carried by the spins but are also influenced by the control of the radial and azimuthal parameters of phase profiles. Therefore, our principle is also applicable to the generation of other spin-multiplexed skyrmion states.

3. Conclusion

In summary, we propose a metasurface scheme for the generation of spin-multiplexed skyrmions, representing an innovative overlap of skyrmions and metaphotonics. This kind of Skyrplate not only requires the metasurface to independently encode the phase with spin states to generate skyrmions but also demands the designed metasurface can be independently modulated when changing the excitation. As a result, skyrmion and skyrmionium are successfully reconstructed under spin-up and spin-down states, respectively. With a simple experimental setup and more compact sizes, further enhance the potential for optical storage. We envision that through the flexible multidimensional control, more topological quasiparticles of light can be generated and manipulated at metasurfaces [49, 50], promoting their application potential in interdisciplinary fields.

Data availability statement

All data that support the findings of this study are included within the article (and any supplementary files).

Acknowledgments

The authors are grateful for supporting with the National Program on Key Basic Research Project of China (2022YFA1404300), National Natural Science Foundation of China (Nos. 12325411, 62288101, 11774162), The Open Research Fund of the State Key Laboratory of Transient Optics and Photonics, Chinese Academy of Sciences (SKLST202218), the Fundamental Research Funds for the Central Universities (020414380175). Postgraduate Research & Practice Innovation Program of Jiangsu Province (KYCX23_0096). C C acknowledges the National Natural Science Foundation of China (No. 62305149).

ORCID iDs

Tianyue Li https://orcid.org/0000-0001-7682-7483
Mengjiao Liu https://orcid.org/0009-0009-8703-1195
Chen Chen https://orcid.org/0000-0003-0599-0798
Xingyi Li https://orcid.org/0000-0001-6339-0729
Shuming Wang https://orcid.org/0000-0002-0191-407X
Shining Zhu https://orcid.org/0000-0002-3472-6497

References

[1] Ozawa T *et al* 2019 *Rev. Mod. Phys.* **91** 015006
[2] Lu L, Joannopoulos J D and Soljačić M 2014 *Nat. Photon.* **8** 821–9
[3] Wang Z, Chong Y, Joannopoulos J D and Soljacic M 2009 *Nature* **461** 772–5
[4] Yang Y, Xu Y F, Xu T, Wang H-X, Jiang J-H, Hu X and Hang Z H 2018 *Phys. Rev. Lett.* **120** 217401
[5] Kim M, Jacob Z and Rho J 2020 *Light Sci. Appl.* **9** 130
[6] Hu Y, Kingsley-Smith J J, Nikkhou M, Sabin J A, Rodriguez-Fortuno F J, Xu X and Millen J 2023 *Nat. Commun.* **14** 2638
[7] Zhou Y, Xu X, Zhang Y, Li M, Yan S, Nieto-Vesperinasd M and Yao B 2022 *Proc. Natl Acad. Sci.* **119** e2209721119
[8] Intaravanne Y, Wang R, Ahmed H, Ming Y, Zheng Y, Zhou Z-K, Li Z, Chen S, Zhang S and Chen X 2022 *Light Sci. Appl.* **11** 302
[9] Bauer T, Banzer P, Karimi E, Orlov S, Rubano A, Marrucci L, Santamato E, Boyd R W and Leuchs G 2015 *Science* **347** 964–6
[10] Lustig E and Segev M 2021 *Adv. Opt. Photonics* **13** 426–61
[11] Li A *et al* 2023 *Nat. Nanotechnol.* **18** 706–20
[12] Shen Y, Zhang Q, Shi P, Du L, Yuan X and Zayats A V 2023 *Nat. Photon.* **18** 15–25
[13] Foster D, Kind C, Ackerman P J, Tai J-S B, Dennis M R and Smalyukh I I 2019 *Nat. Phys.* **15** 655–9
[14] Leslie L S, Hansen A, Wright K C, Deutsch B M and Bigelow N P 2009 *Phys. Rev. Lett.* **103** 250401
[15] Shen Y, Martínez E C and Rosales-Guzmán C 2022 *ACS Photonics* **9** 296–303
[16] Shen Y, Hou Y, Papasimakis N and Zheludev N I 2021 *Nat. Commun.* **12** 5891
[17] Ornelas P, Nape I, de Mello Koch R and Forbes A 2024 *Nat. Photon.* **18** 258–66
[18] Deng Z-L, Shi T, Krasnok A, Li X and Alu A 2022 *Nat. Commun.* **13** 8
[19] Du L, Yang A, Zayats A V and Yuan X 2019 *Nat. Phys.* **15** 650–4
[20] Lei X, Yang A, Shi P, Xie Z, Du L, Zayats A V and Yuan X 2021 *Phys. Rev. Lett.* **127** 237403
[21] Shi P, Lei X, Zhang Q, Li H, Du L and Yuan X 2022 *Phys. Rev. Lett.* **128** 213904
[22] Lin M, Du L and Yuan X 2023 *IEEE Photon. J.* **15** 6500106
[23] Guo C, Xiao M, Guo Y, Yuan L and Fan S 2020 *Phys. Rev. Lett.* **124** 106103
[24] Shen Y, Papasimakis N and Zheludev N I 2024 *Nat. Commun.* **15** 4863
[25] Wu H-J, Yu B-S, Zhu Z-H, Gao W, Ding D-S, Zhou Z-Y, Hu X-P, Rosales-Guzmán C, Shen Y and Shi B-S 2022 *Optica* **9** 187–96
[26] Shen Y 2021 *Opt. Lett.* **46** 3737–40
[27] Liu Z, Wang D, Gao H, Li M, Zhou H and Zhang C 2023 *Adv. Photon.* **5** 034001
[28] He J, Zhao D, Liu H, Teng J, Qiu C-W and Huang K 2023 *Nat. Commun.* **14** 5838
[29] Shen Z, Zhao F, Jin C, Wang S, Cao L and Yang Y 2023 *Nat. Commun.* **14** 1035
[30] Li T, Li X, Yan S, Xu X, Wang S, Yao B, Wang Z and Zhu S 2021 *Phys. Rev. Appl.* **15** 014059
[31] Zhang X, Huang L, Zhao R, Zhou H, Li X, Geng G, Li J, Li X, Wang Y and Zhang S 2022 *Sci. Adv.* **8** eabp8073
[32] Cao G, Lin H and Jia B 2023 *Ultrafast Sci.* **3** 0018
[33] Xu G, Xing H, Xue Z, Lu D, Fan J, Fan J, Shum P P and Cong L 2023 *Ultrafast Sci.* **3** 0033
[34] Fu B, Li T, Zou X, Ren J, Yuan Q, Wang S, Cao X, Wang Z and Zhu S 2022 *J. Phys. D: Appl. Phys* **55** 255105
[35] Li T, Kingsley-Smith J J, Hu Y, Xu X, Yan S, Wang S, Yao B, Wang Z and Zhu S 2023 *Opt. Lett.* **48** 255–8
[36] Li T, Xu X, Fu B, Wang S, Li B, Wang Z and Zhu S 2021 *Photon. Res.* **9** 1062–8
[37] Li X, Zhou Y, Ge S, Wang G, Li S, Liu Z, Li X, Zhao W, Yao B and Zhang W 2022 *Opt. Lett.* **47** 977–80
[38] Li G *et al* 2017 *Nano Lett.* **17** 7974–9
[39] Reineke B, Sain B, Zhao R, Carletti L, Liu B, Huang L, De Angelis C and Zentgraf T 2019 *Nano Lett.* **19** 6585–91
[40] Zhou J, Liu S, Qian H, Li Y, Luo H, Wen S, Zhou Z, Guo G, Shi B and Liu Z 2020 *Sci. Adv.* **6** eabc4385
[41] Huang L, Chen X, Muhlenbernd H, Li G, Bai B, Tan Q, Jin G, Zentgraf T and Zhang S 2012 *Nano Lett.* **12** 5750–5
[42] Devlin R C, Ambrosio A, Rubin N A, Balthasar Mueller J P and Capasso F 2017 *Science* **358** 896–901
[43] Chen C, Gao S, Song W, Li H, Zhu S-N and Li T 2021 *Nano Lett.* **21** 1815–21
[44] Chen C, Xiao X, Ye X, Sun J, Ji J, Yu R, Song W, Zhu S and Li T 2023 *Light Sci. Appl.* **12** 288
[45] Guo X, Li B, Fan X, Zhong J, Qi S, Li P, Liu S, Wei B and Zhao J 2021 *APL Photonics* **6** 086106
[46] Ji J *et al* 2024 *PhotoniX* **5** 13
[47] Li T, Chen Y, Fu B, Liu M, Wang J, Gao H, Wang S and Zhu S 2024 *Laser Photon. Rev.* 2301372
[48] Chen W, Chen Y and Liu W 2019 *Phys. Rev. Lett.* **122** 153907
[49] Shen Y, Yu B, Wu H, Li C, Zhu Z and Zayats A V 2023 *Adv. Photon.* **5** 015001
[50] Zdagkas A, McDonnell C, Deng J, Shen Y, Li G, Ellenbogen T, Papasimakis N and Zheludev N I 2022 *Nat. Photon.* **16** 523–8